HHS Public Access

Author manuscript

Matrix Biol. Author manuscript; available in PMC 2019 April 01.

Published in final edited form as:

Matrix Biol. 2018 April ; 67: 1–14. doi:10.1016/j.matbio.2018.02.022.

Contribution of metabolic disease to bone fragility in MAGP1-deficient mice

S.E. Turecamo[a], **T.A. Walji**[a,b], **T.J. Broekelmann**[c], **J.W. Williams**[d], **S. Ivanov**[e], **N.K. Wee**[a,f], **J.D. Procknow**[a], **M.R. McManus**[a], **G.J. Randolph**[d], **E.L. Scheller**[a,c], **R.P. Mecham**[c], and **C.S. Craft**[a,c]

[a]Medicine, Division of Bone and Mineral Diseases, Washington University School of Medicine, Saint Louis, MO 63110, USA

[b]Department of Molecular Biology, University of Texas Southwestern Medical Center, Dallas, TX 75390, USA

[c]Cell Biology and Physiology, Washington University School of Medicine, Saint Louis, MO 63110, USA

[d]Pathology and Immunology, Washington University School of Medicine, Saint Louis, MO 63110, USA

[e]INSERM U1065, Mediterranean Center of Molecular Medicine, University of Nice Sophia-Antipolis, Faculty of Medicine, Nice, France

[f]Department of Reconstructive Sciences, University of Connecticut Health Center, Farmington, CT 06030, USA

Abstract

Microfibril-associated glycoprotein-1 (MAGP1) is an extracellular matrix protein that interacts with fibrillin and is involved in regulating the bioavailability of signaling molecules such as TGFβ. Mice with germline MAGP1 deficiency (*Mfap2*$^{-/-}$) develop increased adiposity, hyperglycemia, insulin resistance, bone marrow adipose tissue expansion, reduced cancellous bone mass, cortical bone thinning and bone fragility. The goal of this study was to assess whether the *Mfap2*$^{-/-}$ bone phenotypes were due to loss of MAGP1 locally or secondary to a change in whole body physiology (metabolic dysfunction). To do this, mice with conditional deletion of MAGP1 in the limb skeleton were generated by crossing MAGP1-flox mice (*Mfap2*$^{lox/lox}$) with Prx1-Cre mice. *Mfap2*$^{Prx-/-}$ mice did not show any changes in peripheral adiposity, hyperglycemia or insulin sensitivity, but did have increased bone length and cancellous bone loss that was comparable to the germline *Mfap2*$^{-/-}$ knockout. Unlike the germline knockout, marrow adiposity, cortical bone thickness and bone strength in *Mfap2*$^{Prx-/-}$ mice were normal. These findings implicate systemic metabolic dysfunction in the development of bone fragility in germline *Mfap2*$^{-/-}$ mice. An unexpected finding of this study was the detection of MAGP1 protein in the *Mfap2*$^{Prx-/-}$

Correspondence to C.S. Craft: Department of Internal Medicine, Washington University in St. Louis, Campus Box 8301, 425 S. Euclid Ave, Saint Louis, MO 63110, USA. clarissa.craft@wustl.edu.

Supplementary data to this article can be found online at https://doi.org/10.1016/j.matbio.2018.02.022.

The authors declare no conflicts of interest.

hematopoietic bone marrow, despite the absence of MAGP1 protein in osseous bone matrix and absent *Mfap2* transcript expression at both sites. This suggests MAGP1 from a secondary site may accumulate in the bone marrow, but not be incorporated into the bone matrix, during times of regional MAGP1 depletion.

Keywords

MAGP1; Bone; Skeletal fragility; Bone fracture; Diabetes; Obesity; Marrow adipose tissue; Fibrillin; Microfibrils

Introduction

Microfibrils are a component of the ECM, created by the polymerization of fibrillin proteins, that not only provide structural support to tissues, but also are involved in growth factor signaling and interactions with cell-surface receptors (reviewed in [1,2]). Microfibril-associated glycoprotein-1 (MAGP1) is a protein that interacts with microfibrils to influence the bioavailability of signaling molecules (reviewed in [3]). MAGP1 is expressed in most tissues over time, but expression is highest during the neonatal period in interstitial and mesenchymal cells [4]. The C-terminal domain of MAGP1 facilitates binding and incorporation into the matrix, while the N-terminal domain binds and sequesters signaling molecules such as transforming growth factor beta (TGFβ) and bone morphogenetic proteins (BMPs) [5]. The ability of MAGP1 to bind both fibrillin-1 and TGFβ contributes to its role in regulating the signaling level of TGFβ [6–8].

In mice, deficiencies in MAGP1 did not impact structural features of the ECM such as elastic fiber orientation or elastin density [9], however, there were several other phenotypic abnormalities. Mice with germline deletion of *Mfap2*, the gene that expresses MAGP1, have been shown to have altered hematopoiesis, impaired wound healing, skeletal anomalies and metabolic dysfunction [5–7,10,11]. Specifically, MAGP1 deficient mice ($Mfap2^{-/-}$) have increased body weight due to increases in adipocyte size, impaired thermoregulation, and progressive insulin resistance [5,6,11]. The altered metabolic phenotype of $Mfap2^{-/-}$ mice is linked to TGFβ signaling, as treatment with TGFβ neutralizing antibody was able to prevent the development of obesity [6]. Relative to controls, male $Mfap2^{-/-}$ mice have reduced cancellous bone mass by 2-month of age, expansion of marrow adipose tissue by 10-months and altered bone mechanical properties [7,8,10,11]. Spontaneous bone fractures have also been observed in $Mfap2^{-/-}$ mice [5,11].

Individuals with diabetes are known to have increased risk for bone fracture, however, susceptibility cannot be explained by bone mineral density, BMI or glycemic control alone (reviewed by Napoli et al. [12]). The $Mfap2^{-/-}$ mouse is a model of type-II diabetes (T2DM) with bone fragility. To distinguish the consequence of obesity/insulin resistance on bone quality, from loss of MAGP1 in the local bone environment, we generated a mouse in whichMAGP1 was selectively removed from the limb skeleton. Paired related homeobox 1 (*Prrx1, also known as Prx or Prx1*) is expressed in early limb bud mesenchyme [13]. Conditional $Mfap2^{Prx-/-}$ mice showed a similar loss in cancellous bone to the $Mfap2^{-/-}$ mice, but did not develop insulin resistance, excess peripheral adiposity, or an expansion in

MAT. Interestingly, despite a significant reduction in cancellous bone mass, cortical bone thinning and altered mechanical properties found in *Mfap2*$^{-/-}$ mice were not fully recapitulated in *Mfap2*$^{Prx-/-}$ mice. Thus, bone fragility in *Mfap2*$^{-/-}$ mice is likely a secondary complication of metabolic disease and not loss of MAGP1 within the ossified bone matrix.

Results

MAGP1 (Mfap2) gene targeting

To generate *Mfap2*$^{lox/lox}$ mice, *Mfap2*$^{fneo/fneo}$ mice were bred with mice expressing flippase (Flp) which caused excision of the neocassette in the germ line, and restoration of MAGP1 expression while leaving loxP sites flanking exon 2 (Fig. 1A–B). Paired related homeobox 1 (Prx, Prx1) Cre mice were then bred with the *Mfap2*$^{lox/lox}$ mice to cause localized deletion of theMAGP1 in the limbs. As shown in Fig. 1C, Prx1-Cre driven deletion of MAGP1 mRNA (*Mfap2*$^{Prx-/-}$) was efficacious in the femurs of both male and female mice. Cre-driven loss of MAGP1 protein expression from the limbs was also confirmed *via* Western blot using tibia protein lysates (Fig. 1D). Depletion of *Mfap2* mRNA (MAGP1) occurred in both the calcified bone and flushed marrow (Fig. 1E). Expression of *Mfap2* in the lung and gonadal white adipose tissue (gWAT) was unaffected by the Prx1-Cre. However, in agreement with previously published literature [14], *Mfap2* (MAGP1) was targeted in the inguinal white adipose tissue (iWAT) of Prx1-Cre expressing mice (Fig. 1E).

Using micro-computed tomography (μCT), Combs et al. [15] demonstrated that MAGP2-knockout mice show no osteopenia, and loss of MAGP2 in tandem with MAGP1 (MAGP1/MAGP2 double knockout mouse) does not exacerbateMAGP1-knockout osteopenia. Therefore, it is unlikely thatMAGP2 can partially compensate for MAGP1 loss. However, expression of *Mfap5* (MAGP2) transcript was still assessed in *Mfap2*$^{Prx-/-}$ bones. As expected, *Mfap5* (MAGP2) mRNA expression was unaffected by Prx1-Cre mediated deletion of *Mfap2* (MAGP1) (Fig. 1F).

Prx1-targeted MAGP1 deficiency does not affect adiposity

The goal of this project was to determine whether loss of MAGP1 locally (within the bone) or metabolic dysfunction (obesity/diabetes) was the cause of bone fragility observed in the germline MAGP1-deficient mice. Therefore, an extensive metabolic profile was generated for the *Mfap2*$^{Prx-/-}$ mice to confirm they lacked an obese-diabetic phenotype. The body composition of the *Mfap2*$^{Prx-/-}$ mice was measured by EchoMRI scan. At 3-months, 6-months, and 10-months, there was no significant difference in the body weight or whole body fatmass between the *Mfap2Prx*−/− group and the wild type control group in either male (Fig. 2A) or female mice (Supplemental Fig. 1A). Whole body lean muscle mass was slightly reduced at 6- and 10-months in Prx1-Cre; *Mfap2*$^{f/f}$ male mice, relative to WT. Female *Mfap2*$^{Prx-/-}$ mice lean mass was normal at all time points. Tissue weights were also measured (Fig. 2B, Supplemental Fig. 1B). Gonadal WAT, brown adipose tissue (BAT), liver, and spleen weights were unchanged relative to controls in *Mfap2*$^{Prx-/-}$ mice. Despite a lack of MAGP1 mRNA in the iWAT – *Mfap2*$^{Prx-/-}$ iWAT weights were indistinguishable from WT.

Glucose metabolism is normal in Prx1-targeted MAGP1 deficiency

Adult *Mfap2*$^{-/-}$ mice are insulin-resistant and glucose intolerant [6,8,11]. To assess glucose metabolism in *Mfap2*$^{Prx-/-}$ mice, insulin tolerance tests (ITTs) and glucose tolerance tests (GTTs) were performed. Unlike *Mfap2*$^{-/-}$ mice, there were no significant differences in the fasting glucose levels between *Mfap2*$^{Prx-/-}$ and wild type mice in either male or female mice at the ages of 3-, 6-, or 10-months (Fig. 3A–C, Supplemental Fig. 2A–C). Male *Mfap2*$^{Prx-/-}$mice have normal insulin sensitivity at all time points, and do not develop insulin resistance like the germline-MAGP1-deficient (*Mfap2*$^{-/-}$) mice (Fig. 3A–C). At individual time points during the ITT, female *Mfap2*$^{Prx-/-}$ mice were slightly more insulin sensitive than WT female mice at 3- and 6-months. However, comparison of the ITT curves by ANOVA analysis revealed no statistical significance between the genotypes for all ages (Supplemental Fig. 2A–C). The glucose clearing capacity, as measured by GTT, of male and female *Mfap2*$^{Prx-/-}$ mice was unchanged relative to controls at all ages (Fig. 3A–C, Supplemental Fig. 2A–C). In total, the obese-diabetic phenotypes observed in the *Mfap2*$^{-/-}$ mice were absent in the *Mfap2*$^{Prx-/-}$ mice.

Prx1-targeted MAGP1 deficiency results in increased bone length and reduced bone mass

Germline MAGP1 deficiency in mice causes modest increases in long bone length and significantly reduced bone mass [7,8,10,11]. Tibia lengths of *Mfap2*$^{Prx-/-}$ mice were measured by digital caliper, and bone mass and architecture were quantified by micro-computed tomography (μCT). Both male and female *Mfap2*$^{Prx-/-}$ mice had modest, but statistically significant increases in tibia length (~0.5 mm, +3%; Fig. 4A, Supplemental Fig. 3A). Relative to WT, cancellous bone mass (bone volume/total volume, BV/TV) and bone mineralization (BMD) in male *Mfap2*$^{Prx-/-}$ mice were trending toward loss by age 3-months and were significantly less at 6- and 10-months of age (Fig. 4B–C). Percent cancellous bone loss (−30% for BV/TV) in *Mfap2*$^{Prx-/-}$ mice is comparable to that previously observed in *Mfap2*$^{-/-}$ mice [8,11]. Cortical bone mineral density and thickness of *Mfap2*$^{Prx-/-}$ tibias was comparable to WT (Fig. 4D–E). Bone marrow adiposity was determined by μCT imaging of osmium-stained-decalcified tibias. In contrast to *Mfap2*$^{-/-}$ mice, which had a significant (5-fold) increase in marrow adiposity at 10-months of age [11], bone marrow adiposity was unchanged by local depletion of MAGP1 expression by Prx1-Cre (Fig. 4F–G). All parameters acquired by μCT of cancellous and cortical bone are shown in Table 1 (cancellous) and Table 2 (cortical).

Depletion of *Mfap2* mRNA (MAGP1) in the bones of male and female *Mfap2*$^{Prx-/-}$ mice was comparable (Fig. 1C). Despite this, unlike the males, female *Mfap2*$^{Prx-/-}$ mice did not have a reduced bone mass phenotype (Supplemental Fig. 3B–C). Female *Mfap2*$^{Prx-/-}$ cortical bone mineral density, cortical bone thickness, and bone marrow adiposity were also comparable to control mice (Supplemental Fig. 3D–F).

Bone strength is unaffected by bone-targeted deletion of MAGP1

Mice with germline MAGP1 deficiency in both inbred and outbred strains develop spontaneous bone fractures [5,11]. Mechanical testing was performed using femurs from *Mfap2*$^{Prx-/-}$, *Mfap2*$^{-/-}$ and control mice to evaluate whether loss of bone-specific expression of MAGP1 (and corresponding reduction in bone mass) is sufficient to render the bones

more susceptible to failure, or whether the underlying metabolic dysfunction in germline MAGP1 knockout mice causes the observed bone fragility. Fig. 5 shows a comparison of the mechanical properties of *Mfap2*$^{Prx-/-}$ femurs to germline *Mfap2*$^{-/-}$ and WT femurs. The yield load, maximum load, work to fracture and stiffness was unchanged in *Mfap2*$^{Prx-/-}$ femurs, suggesting bone fragility in *Mfap2*$^{-/-}$ bones is a secondary complication rather than the direct consequence of local MAGP1 depletion. Supplemental Fig. 4 compares the femoral mechanical properties of the same inbred *Mfap2*$^{Prx-/-}$ mice to a second *Mfap2*$^{-/-}$ germline knockout line (BlackSwiss, outbred); showing again that germline but not local MAGP1 loss is required for the development of bone fragility.

Altered immunity in Mfap2$^{-/-}$ mice is not maintained in Mfap2$^{Prx-/-}$ mice

Hematopoiesis in *Mfap2*$^{Prx-/-}$ and *Mfap2*$^{-/-}$ animals was assessed at the age of 3-months. This time point was originally chosen because reduced bone mass is appreciable, but the *Mfap2*$^{-/-}$ mice are neither obese nor pre-diabetic. In MAGP1 germline knockout mice, neutrophil and monocyte levels in blood are significantly reduced (50% and 45% respectively, Fig. 6 and Table 3). In contrast, *Mfap2*$^{Prx-/-}$male and female mice have a normal distribution of myeloid and lymphoid cells in whole blood (Fig. 6 and Table 3). The frequency of hematopoietic precursor cells in *Mfap2*$^{Prx-/-}$ bone marrow samples was also unchanged relative to controls (Table 4).

MAGP1 protein accumulates in Mfap2$^{Prx-/-}$ mice

Given the observed depletion of *Mfap2* transcript in bone marrow (Fig. 1E), the lack of a hematopoietic phenotype in the femur was unexpected. In response, marrow-depleted bone, whole bone marrow and lung (positive control) samples were evaluated for MAGP1 protein content (Fig. 7). Tissues were collected from Jackson Laboratories C57BL/6 J (positive control), *Mfap2*$^{-/-}$ mice (negative control), Cre-negative-*Mfap2*$^{lox/lox}$ mice (positive control) and *Mfap2*$^{Prx-/-}$ mice (male and female). As expected, MAGP1 protein was present in all C57BL/6 J and Cre-negative tissues, and absent in all *Mfap2*$^{-/-}$ tissues. Prx1-Cre efficiency was confirmed by the absence of detectable MAGP1 protein expression in marrow-depleted femurs. Unexpectedly, MAGP1 protein was detectable, at near WT levels, in *Mfap2*$^{Prx-/-}$ whole bone marrow samples; introducing the possibility that MAGP1 protein from a secondary source may accumulate in the bone marrow matrix of *Mfap2*$^{Prx-/-}$ mice, but is not incorporated into the ossified bone matrix. Restoration of MAGP1 protein in the bone marrow may explain why *Mfap2*$^{Prx-/-}$ mice do not develop a hematopoietic phenotype.

Discussion

Mice with germline MAGP1 deficiency have been previously reported to be obese with fragile bones [5,10,11]. In this study, mice with conditional MAGP1 deficiency in the limb were evaluated to determine the role of MAGP1 in the bone microenvironment specifically. Despite Prx1 expression in iWAT, and subsequent *Mfap2* transcript deletion, these mice did not have an increase in iWAT mass nor develop the documented metabolic dysfunction that is present in the germ line *Mfap2*$^{-/-}$ mouse; allowing distinction of the role of diabetic pathophysiology from local MAGP1 expression on skeletal health. Both *Mfap2*$^{-/-}$ and *Mfap2*$^{Prx-/-}$ mice have a significant decrease in cancellous bone volume indicating that the

local bioavailability of MAGP1 in the bone matrix is a key player in the bone remodeling process. Tibia bone length is increased in both *Mfap2*$^{-/-}$ and *Mfap2*$^{Prx-/-}$ mice. Cortical bone mineral density is unaffected by either global or local MAGP1 depletion in c57BL/6 mice. However, yield load, max load and work to fracture are reduced in *Mfap2*$^{-/-}$ mice but are normal in *Mfap2*$^{Prx-/-}$ mice. We postulate that the development of metabolic disease (hyperglycemia, insulin resistance, obesity) that occurs in *Mfap2*$^{-/-}$ mice, but not *Mfap2*$^{Prx-/-}$ mice, plays a key role in the development of bone fragility in the global knockout mice. Diabetes is considered a risk factor for bone fractures. It is well established that diabetes-associated bone fragility cannot be predicted by bone mineral density alone. Reduced bone turnover, glycation of the bone matrix, and architectural changes have been implicated in altering the mechanical properties of bone in diabetic patients [12]. Comparison of c57BL/6 germline knockout [11] and Prx1-conditional knockout mice revealed an important distinction between the diabetic *Mfap2*$^{-/-}$ and non-diabetic *Mfap2*$^{Prx-/-}$ mice which may explain the *Mfap2*$^{-/-}$-associated bone fragility phenotype. Specifically, despite loss of MAGP1 protein in the cortical bone of both *Mfap2*$^{-/-}$ and *Mfap2*$^{Prx-/-}$ mice, cortical bone thinning occurs only in the diabetic *Mfap2*$^{-/-}$ mice [11].

Interestingly, a sexual dimorphism in the cancellous bone mass phenotype was observed *Mfap2*$^{Prx-/-}$ mice. *Mfap2*$^{Prx-/-}$ male mice displayed significantly reduced cancellous bone while bone mass in female *Mfap2*$^{Prx-/-}$ mice was comparable to Cre-negative controls. By contrast, both male and female *Mfap2*$^{Prx-/-}$ mice had a slight, but significant, increase in long bone length. Quantitative PCR and Western blot confirmed that both MAGP1 transcript and protein were targeted by the Prx1-Cre. These findings do not match with the bone phenotype of female *Mfap2*$^{-/-}$ mice, which were previously reported to have cancellous bone loss [7]. The reason for this discrepancy is unknown, however, it is worth noting that in the previous report the female germline knockout mice were on an outbred Black Swiss background while the *Mfap2*$^{Prx-/-}$ female mice are inbred C57BL/6J.

An unexpected and confounding finding of this study was the accumulation of MAGP1 protein in the isolated bone marrow of *Mfap2*$^{Prx-/-}$ mice. Initial characterization of the *Mfap2*$^{Prx-/-}$ animals demonstrated that mRNA expression of MAGP1 was efficiently targeted in both osseous marrow-depleted bone and isolated bone marrow. Western blot of whole bone lysates using a MAGP1-specific antibody provided further confirmation of our conditional deletion of MAGP1. However, the absence of the two marrow-relevant phenotypes – monocytopenia/neutropenia and bone marrow adipocyte expansion – was unexpected. The lack of a marrow fat phenotype could be explained by the absence of an obese-diabetic state, lack of an immune cell phenotype, which is apparent prior to the obesity/diabetes phenotype in the germline knockout, warranted further investigation. In response, protein lysate preparations of isolated whole bone marrow were compared to the marrow-depleted femurs by Western blot. Indeed, near WT levels of MAGP1 protein were detectable in *Mfap2*$^{Prx-/-}$ isolated bone marrow, but completely absent in marrow-depleted bone samples. The significant accumulation of MAGP1 protein, despite the lack of mRNA transcript, introduces the possibility that MAGP1 protein from a secondary source can accumulate in the bone marrow matrix of *Mfap2*$^{Prx-/-}$ mice. Localization of MAGP1 protein in the bone marrow milieu was attempted by immunohistochemistry, however, despite

optimization efforts the non-specific staining of theMAGP1antibody could not be eliminated.

Incorporation of MAGP1 from a distant site into the bone marrow may be feasible given the bone marrow's dense vascular network. While future work is needed to explore the source of marrow-localized MAGP1 in *Mfap2*$^{Prx-/-}$ mice, support for transportation of MAGP1 in circulation exists. Werneck et al. [9] showed that full length recombinant MAGP1 can be injected into the tail vein of mice, and that this circulating recombinant MAGP1 has biological function. Specifically, tail vein administration of full length MAGP1 reduced thrombotic occlusion time in the carotid artery following vascular injury, and importantly the recombinant MAGP1 was found localized to the internal elastic lamina at the site of injury. Werneck et al. [9] also showed that recombinant MAGP1 is capable of physical interaction with plasma proteins, including fibrinogen and von Willebrand factor.

The molecular weight of MAGP1 protein isolated from *Mfap2*$^{Prx-/-}$ whole bone marrow samples is consistent with full length MAGP1, and is the same size as MAGP1 protein isolated from osseous bone matrix. This suggests that MAGP1 protein accumulating in *Mfap2*$^{Prx-/-}$ bone marrow contains MAGP1's matrix binding domain, and is therefore likely to incorporate into the loose network of ECM structures within the bone marrow. MAGP1 is a constitutive component of fibrillin-1-rich microfibrils [16]. Global deficiencies in either MAGP1 or fibrillin-1 results in increased long bone length, and reduced bone mass that is downstream of enhanced osteoclastogenesis [2,17,18]. It was recently shown that fibrillin-1 microfibrils have an important role in bone marrow ECM. Specifically, immunofluorescence was used to localize fibrillin-1 to stem cell niches, and Prx1-Cremediated loss of fibrillin-1 (*Fbn1*$^{Prx-/-}$) modified skeletal stem cell fate, erythroid expansion, and HSC maintenance [19,20]. The presence ofMAGP1'smajor binding partner - fibrillin-1 - within the bone marrow provides an ideal docking station for MAGP1 protein in *Mfap2*$^{Prx-/-}$ mice.

In summary, the *Mfap2*$^{Prx-/-}$ model of local MAGP1 deficiency was used to demonstrate that MAGP1 incorporation into bone matrix contributes to bone mass but does not directly contribute to the mechanical properties of the bone. Instead, the obese and prediabetic state of *Mfap2*$^{-/-}$ mice likely results in a reduction in bone quality, independent of bone mass or MAGP1 expression. Future work is needed to test whether rescue of the diabetic phenotype in *Mfap2*$^{-/-}$ mice is sufficient to prevent bone fragility.

Experimental procedures

Animals and diets

Male and female mice were maintained on a C57BL/6J background, housed in a pathogen-free animal facility and fed standard chow *ad libitum*. All animals were treated in accordance with animal protocols approved by the Animal Studies Committee at Washington University.

Generation of Mfap2$^{-/-}$ mice

MAGP1-deficient mice were generated using C57BL/6 N-derived ES cells [*Mfap2*$^{tm1a(KOMP)Wtsi}$] purchased from KOMP Repository (#EPD0224_1_H08). ES cells

were injected into blastocyst from C57BL/6J donors and transferred into pseudopregnant C57BL/6J females. Offspring were maintained on the Jackson Laboratories C57BL/6J strain.

Generation of Mfap2$^{Prx-/-}$ mice

The germline *Mfap2*$^{-/-}$ line ("gKO") was crossed with a C57BL/6N background mouse line heterozygous for the flippase (Flp) recombinase transgene for one generation (UC Davis Mutant Mouse Regional Resource Center, #036512-UCD). The Flp recombinase cuts the cMAGP1 allele at the flippase recognition target (FRT) sites that flank the neomycin cassette, thereby restoring expression to the *Mfap2* gene (Fig. 1A). The Flp transgene was then bred out of the colony. Females from the Flp-negative cMAGP1 line ("Flp'd") were then crossed with male Prx1-Cre mice with a C57BL/6J background (The Jackson Laboratory, #005584). In mice possessing the Prx1-Cre allele, Cre recombinase is expressed in cells that express *Prx1* in the embryonic mesoderm. The Cre recombinase targets the 5′ and 3′ loxP sites that flank the *Mfap2* allele (Fig. 1A). Therefore, in cells that express *Prx1* during development, the *Mfap2* allele is removed ("Cre'd"). Generation of *Mfap2*$^{Prx-/-}$ mice was confirmed by isolation of genomic DNA (gDNA) from the tibias of mice WT, gKO, Flp'd, and Cre'd lines. PCR amplification of the gDNA was conducted using wt-MAGP1 primers, mut-MAGP1 primers, and Cre primers. WT-MAGP1 forward primer sequence is 5′-ATGGGCCAGGGGTAGACAGGATTG-3′, reverse is 5′-TAGGCACCCCGCATAGGAAGGACT-3′. Mut-MAGP1 forward primer sequence is 5′-CTCACCTCCTCCAGCTCTTACTCC-3′, reverse is 5′-AATCCCGTCCCCCTTCCTATGT-3′. Cre forward primer sequence is 5′-GCGGTCTGGCAGTAAAAACTATC-3′, reverse is 5′-GTGAAACAGCATTGCTGTCACTT-3′.

Body composition

Longitudinal whole body composition was determined using the EchoMRI 3-in-1 model instrument (Echo Medical Systems) at ages 3-months, 6-months and 10-months. At each age, mice were scanned twice in the EchoMRI to quantify body fat, free water, and lean (muscle) content. The results from each scan were averaged.

Insulin and glucose tolerance testing

For both insulin tolerance tests (ITTs) and glucose tolerance tests (GTTs), mice were housed individually on aspen bedding and fasted for 6 h. At the beginning of the fast, each mouse was weighed and a small piece of its tail was cut. After the six hour fast, the tail blood baseline glucose of each mouse was measured using Contour strips and meters (Bayer). For ITTs, each mouse then received an intraperitoneal injection of 0.75 U/kg Humulin-R insulin (Lilly). For GTTs, each mouse received an intraperitoneal injection of 1.0 mg/g of dextrose. For both ITTs and GTTs, the tail blood glucose of each mouse was measured at 30, 60, 90, and 120 min after the injection. Longitudinal ITTs and GTTs experiments were conducted at ages 3-months, 6-months and 10-months.

Tissue collection

The tissues of the *Mfap2*$^{Prx-/-}$ mice were harvested at 10-months. Mouse fur was sprayed with 70% EtOH, then inguinal white adipose tissue (iWAT), gonadal white adipose tissue (gWAT), brown adipose tissue (BAT), liver, spleen, and tibias were collected. The soft tissues were rinsed in phosphate-buffered saline (PBS), blotted dry, and weighed. Tissues were fixed in 10% neutral buffered formalin for 24-h then stored in PBS or snap frozen in liquid nitrogen. To collect the marrow depleted femur and whole bone marrow samples the proximal portion of the femur was removed then placed in a collection tube in which the femur remained elevated over a second tube. With gentle centrifugation (1600*g* for 1 min) the marrow passed through a small hole in tube one and collected in tube two below. The remaining portion of the femur and the marrow pellet were then snap frozen. Tibia length was determined using a digital caliper (Mitutoyo).

Micro-computed tomography and osmium staining

Longitudinal micro-computed tomography (CT) experiments were conducted at ages 3-months, 6-months and 10-months. *In vivo* micro-computed tomography of the tibias was conducted at 3- and 6-months. Each mouse was anesthetized using 2% isoflurane and taped down to scan the right tibia using a Scanco VivaCT40 (Scanco Medical AG) at 20 μm voxel resolution. After the scan was complete, the mouse was removed from the machine and allowed to wake under a warming light. *Post mortem* micro-computed tomography (μCT) was completed on tibias from the same mice at 10-month-old. Bones were fixed in 10% neutral buffered formalin and then embedded in 2% agarose gel. *Post mortem* tibias were also scanned at 20 μm voxel resolution, using a Scanco μCT 40 (Scanco Medical AG) calibrated using a hydroxyapatite phantom. Measurements of both cancellous and cortical bones were made based on reported guidelines [21]. For cancellous bone, 50 slices (1 mm) below the growth plate were contoured to exclude the cortical bone, allowing cancellous bone volume/tissue volume (BV/TV) and bone mineral density (BMD) to be determined. For cortical bone, 20 slices (400 μm) located 2 mm proximal to the tibia–fibula junction were analyzed to determine cortical tissue mineral density (TMD) and cortical bone thickness. A threshold of 260 for cortical bone (on a 0–1000 scale) was maintained. For cancellous bone, a threshold of 175 was used for μCT and 180 for vivaCT. Tibias from 10-month-old mice were then decalcified in 14% EDTA for 3-weeks. Demineralized bones were incubated in a solution containing 1% osmium and 2.5% potassium dichromate for 48-h at room temperature. After thorough washing (water) and overnight storage in PBS, tibias were embedded in 1% agarose gel. Osmium stained bones were then scanned as above, using a Scanco μCT 40, but at 10 μm voxel resolution. Analysis was performed in the same region of interest as the cancellous bone (100 slices to achieve 1 mm total, distal to the growth plate), using a threshold of 350 (on a 0–1000 scale). Osmium volume (OV) is quantification of the total OV within the region of interest. OV/TV is division of the OV by the volume of the marrow cavity within the same region, as calculated from the cancellous bone analysis.

Histology

Tissues were fixed in 10% buffered formalin, dehydrated by an ethanol gradient, and stored in 70% ethanol at 4 °C before paraffin embedding. Five-micron tissue sections were stained with hematoxylin and eosin. Images were taken using an Olympus Nanozoomer 2.0-HT System with NDP. scan 2.5 image software.

Bone mechanical testing

Upon dissection at 10-months of age, femurs were wrapped in PBS-soaked gauze and stored at −20 °C. For testing, femurs were thawed in PBS for 1 h prior to use, and testing was carried out at room temperature using a servohydraulic testing machine (8841 Dynamite, Instron). Femurs were positioned on two supports 7 mm apart, and the central loading point was mid-diaphysis. Displacement was applied transverse to the long axis of the bone at a rate of 0.01 mm/s until failure. Force-displacement data were recorded at 60 Hz and analyzed to determine measures of stiffness and whole bone strength.

Flow cytometry

Blood samples were collected from the superficial temporal vein, by puncture with a 20G needle and collected directly into 10 μL of 100 mM EDTA solution to prevent coagulation. Bone marrow was isolated by flushing bones with 20G needle and single cell suspensions prepared by disruption by pipeting. Red blood cells were lysed (Pharmlyse, BD Biosciences) following manufacturer's instructions and samples were counted (Cellometer ×4, Nexcelom Biosciences) and processed for staining. Samples were FcR-blocked (2.4G2, Biolegend) then stained on ice with specific antibodies; CD11b APC-Cy7 conjugated (M1/70, BD biosciences), CD115 APC conjugated (AFS98, eBioscience), Ly6C PerCP-Cy5.5 conjugated (HK1.4, Biolegend), Ly6G FITC conjugated (1A8, BD Biosciences), and CD43 PE conjugated (1B11, Biolegend), CD117 Fitc conjugated (c-Kit) (2B8, BD Biosciences), CD135 (Flt3) PE conjugated (A2F10, Biolegend), Sca1 PerCP Cy5.5 conjugated (D7, eBioscience), CD45 Pacific Blue conjugated (30-Fl1, Biolegend), SiglecF PE conjugated (E50-2440, BD Biosciences), TCRβ Fitc conjugated (H57-597, eBioscience), CD19 PEcy7 conjugated (6D5, Biolegend), CD4 PE conjugated (GK1.5, eBioscience), CD8 PerCPCy5.5 conjugated (53-6.7, Biolegend). Samples were run on a BD LSRFortessa instrument and analysis performed using FlowJo V10 (Treestar). Cell populations were identified using the following gating strategy. For blood CD45+ cells, monocyte (Ly6G−, CD115+, CD11b+; then separated into Ly6C+ and Ly6C− populations), neutrophil (CD11b+, Ly6G+), T cell (TCRβ+; then separated into CD4+ and CD8+ populations), B cell (CD19+), eosinophil (Siglec F+ CD11b+). For bone marrow: MDP (Ly6G−, CD11b− CD135+ CD117+ Sca1− CD115+), CDP (Ly6G− CD11b− CD135+ CD117− CD115+), MP (Ly6G− CD11b− Flt3+ CD117+ Sca1− CD115−), PreDC (Ly6G− CD11b− Flt3+ CD11c+), Neutrophil (Ly6G+ CD11b+), Monocyte (Ly6G− CD115+ CD11b+, then separated into Ly6C+ and Ly6C− populations). Flow cytometry experiments for *Mfap2*$^{Prx-/-}$ mice and *Mfap2*$^{-/-}$ mice were conducted at different times.

Western blot

Tissue samples were pulverized in liquid nitrogen, then extracted with 1× Laemmli SDS sample buffer containing 10 mM DTT at a ratio of 40 μL per mg for bones and 80 μL/mg for lung and bone marrow. The samples were heated at 100 °C for 5 min, stored for 2 h room temperature, reheated for 2 min at 100 °C, then spun for 2 min in a micro-centrifuge before loading into 10% SDS-PAGE gels. The gels were loaded with 30 μL per lane for bones, 15 μL per lane for bone marrow and 5 μL per lane for lung. Following separation, proteins were transferred to nitrocellulose membranes and stained with Ponceau to confirm protein loading and transfer. The membranes were washed of stain and blocked for 1 h in HEPES buffered saline containing 0.02% Tween-20 with 1% nonfat dried milk, 1% BSA, and 1% Teleostean gelatin (Millipore Sigma) pH 7.4 then incubated overnight in blocking solution with 1:2000 diluted MAGP1 primary antibody. Bound MAGP-1 antibody was detected with HRP-conjugated secondary antibodies (GE Healthcare) then visualized with chemiluminescent HRP substrate (Millipore).

MAGP1 antibody

A polyclonal antibody was generated by immunizing rabbits with front half of MAGP-1 protein expressed and purified as aGST-fusion protein. Affinity pure anti-MAGP-1 IgG was then isolated from the anti-sera using the front half of MAGP-1 expressed and purified as a 6HIS-tagged fusion protein [5,15].

RNA extraction and quantitative RT-PCR

Frozen tissue samples were pulverized using a TissueLyser or Braun Mikrodismembrator then RNA extracted in Trizol (Invitrogen) with chloroform and further purified by alcohol precipitation (Fig. 1C) or using Qiagen RNeasy columns (Fig. 1E–F). RNA was reverse transcribed using Life Technologies RNA-to-cDNA reverse transcription kits. Quantitative PCR was performed using Taqman primer-probe sets and Taqman universal master mix (Applied Biosystem). Transcript levels (relative units, RU), normalized to either *Rplpo* (36B4) or cyclophilin (PPIA), were determined by the equation, $1/2^{\Delta CT}$.

Statistical analysis

Statistical comparisons were performed using Graphpad Prism® (GraphPad Software, Inc.). Student's *t*-test was used for single comparisons, one-way ANOVA formultiple comparisons, or two-way ANOVA for repeated-measures. Results with a p value ≤ 0.05 were considered statistically significant.

Supplementary Material

Refer to Web version on PubMed Central for supplementary material.

Acknowledgments

This work was supported by National Institutes of Health grants HL-053325 and HL-105314 to RPM, and K99-DE024178 and R00-DE024178 to ELS, the American Diabetes Association grant 7-13-JF-16 to CSC, and awards from the Washington University Nutrition and Obesity Research Center and Washington University Musculoskeletal Research Center to CSC. Technical support was provided by Washington University's Nutrition

and Obesity Research Center (grant P30-DK-056341), Diabetes Research Center (P30 DK020579), and Musculoskeletal Research Center (P30-AR-057235).

Abbreviations used

ECM	extracellular matrix
MAT	marrow adipose tissue
MAGP1	microfibril-associated glycoprotein-1
TGFβ	transforming growth factor beta
Fbn	fibrillin
Prx1	paired related homeobox-1

References

1. Ramirez F, Carta L, Lee-Arteaga S, Liu C, Nistala H, Smaldone S. Fibrillin-rich microfibrils - structural and instructive determinants of mammalian development and physiology. Connect. Tissue Res. 2008; 49:1–6. DOI: 10.1080/03008200701820708 [PubMed: 18293172]
2. Smaldone S, Ramirez F. Fibrillin microfibrils in bone physiology. Matrix Biol. 2016; 52–54:191–197. DOI: 10.1016/j.matbio.2015.09.004
3. Mecham RP, Gibson MA. The microfibril-associated glycoproteins (MAGPs) and the microfibrillar niche. Matrix Biol. 2015; 47:13–33. DOI: 10.1016/j.matbio.2015.05.003 [PubMed: 25963142]
4. Chen Y, Faraco J, Yin W, Germiller J, Francke U, Bonadio J. Structure, chromosomal localization, and expression pattern of the murine Magp gene. J. Biol. Chem. 1993; 268:27381–27389. [PubMed: 8262979]
5. Weinbaum JS, Broekelmann TJ, Pierce RA, Werneck CC, Segade F, Craft CS, et al. Deficiency in microfibril-associated glycoprotein-1 leads to complex phenotypes in multiple organ systems. J.Biol. Chem. 2008; 283:25533–25543. DOI: 10.1074/jbc.M709962200 [PubMed: 18625713]
6. Craft CS, Pietka TA, Schappe T, Coleman T, Combs MD, Klein S, et al. The extracellular matrix protein MAGP1 supports thermogenesis and protects against obesity and diabetes through regulation of TGF-β. Diabetes. 2014; 63:1920–1932. DOI: 10.2337/db13-1604 [PubMed: 24458361]
7. Craft CS, Broekelmann TJ, Zou W, Chappel JC, Teitelbaum SL, Mecham RP. Oophorectomy-induced bone loss is attenuated in MAGP1-deficient mice. J. Cell. Biochem. 2012; 113:93–99. DOI: 10.1002/jcb.23331 [PubMed: 21898536]
8. Walji TA, Turecamo SE, DeMarsilis AJ, Sakai LY, Mecham RP, Craft CS. Characterization of metabolic health in mouse models of fibrillin-1 perturbation. Matrix Biol. 2016; 55:63–76. DOI: 10.1016/j.matbio.2016.02.006 [PubMed: 26902431]
9. Werneck CC, Vicente CP, Weinberg JS, Shifren A, Pierce RA, Broekelmann TJ, et al. Mice lacking the extracellular matrix protein MAGP1 display delayed thrombotic occlusion following vessel injury. Blood. 2008; 111:4137–4144. DOI: 10.1182/blood-2007-07-101733 [PubMed: 18281502]
10. Craft CS, Zou W, Watkins M, Grimston S, Brodt MD, Broekelmann TJ, et al. Microfibril-associated glycoprotein-1, an extracellular matrix regulator of bone remodeling. J. Biol. Chem. 2010; 285:23858–23867. DOI: 10.1074/jbc.M110.113019 [PubMed: 20501659]
11. Walji TA, Turecamo SE, Sanchez AC, Anthony BA, Abou-Ezzi G, Scheller EL, et al. Marrow adipose tissue expansion coincides with insulin resistance in MAGP1-deficient mice. Front. Endocrinol. 2016; 7:87.doi: 10.3389/fendo.2016.00087
12. Napoli N, Chandran M, Pierroz DD, Abrahamsen B, Schwartz AV, Ferrari SL, et al. Mechanisms of diabetes mellitus-induced bone fragility. Nat. Rev. Endocrinol. 2017; 13:208–219. DOI: 10.1038/nrendo.2016.153 [PubMed: 27658727]

13. Logan M, Martin JF, Nagy A, Lobe C, Olson EN, Tabin CJ. Expression of Cre Recombinase in the developing mouse limb bud driven by a Prxl enhancer. Genesis. 2002; 33:77–80. DOI: 10.1002/gene.10092 [PubMed: 12112875]

14. Sanchez-Gurmaches J, Hsiao W-Y, Guertin DA. Highly selective in vivo labeling of subcutaneous white adipocyte precursors with Prx1-Cre. Stem Cell Reports. 2015; 4:541–550. DOI: 10.1016/j.stemcr.2015.02.008 [PubMed: 25801508]

15. Combs MD, Knutsen RH, Broekelmann TJ, Toennies HM, Brett TJ, Miller CA, et al. Microfibril-associated glycoprotein 2 (MAGP2) loss of function has pleiotropic effects in vivo. J. Biol. Chem. 2013; 288:28869–28880. DOI: 10.1074/jbc.M113.497727 [PubMed: 23963447]

16. Henderson M, Polewski R, Fanning JC, Gibson MA. Microfibril-associated glycoprotein-1 (MAGP-1) is specifically located on the beads of the beaded-filament structure for fibrillin-containing microfibrils as visualized by the rotary shadowing technique. J. Histochem. Cytochem. 1996; 44:1389–1397. [PubMed: 8985131]

17. Nistala H, Lee-Arteaga S, Smaldone S, Siciliano G, Ramirez F. Extracellular microfibrils control osteoblast-supported osteoclastogenesis by restricting TGF{beta} stimulation of RANKL production. J. Biol. Chem. 2010; 285:34126–34133. DOI: 10.1074/jbc.M110.125328 [PubMed: 20729550]

18. Nistala H, Lee-Arteaga S, Smaldone S, Siciliano G, Carta L, Ono RN, et al. Fibrillin-1 and -2 differentially modulate endogenous TGF-β and BMP bioavailability during bone formation. J. Cell Biol. 2010; 190:1107–1121. DOI: 10.1083/jcb.201003089 [PubMed: 20855508]

19. Smaldone S, Bigarella CL, Del Solar M, Ghaffari S, Ramirez F. Fibrillin-1 microfibrils influence adult bone marrow hematopoiesis. Matrix Biol. 2016; 52–54:88–94. DOI: 10.1016/j.matbio.2015.11.006

20. Smaldone S, Clayton NP, del Solar M, Pascual G, Cheng SH, Wentworth BM, et al. Fibrillin-1 regulates skeletal stem cell differentiation by modulating TGFβ activity within the marrow niche. J. Bone Miner. Res. 2016; 31:86–97. DOI: 10.1002/jbmr.2598 [PubMed: 26189658]

21. Bouxsein ML, Boyd SK, Christiansen BA, Guldberg RE, Jepsen KJ, Müller R. Guidelines for assessment of bone microstructure in rodents using micro-computed tomography. J. Bone Miner. Res. 2010; 25:1468–1486. DOI: 10.1002/jbmr.141 [PubMed: 20533309]

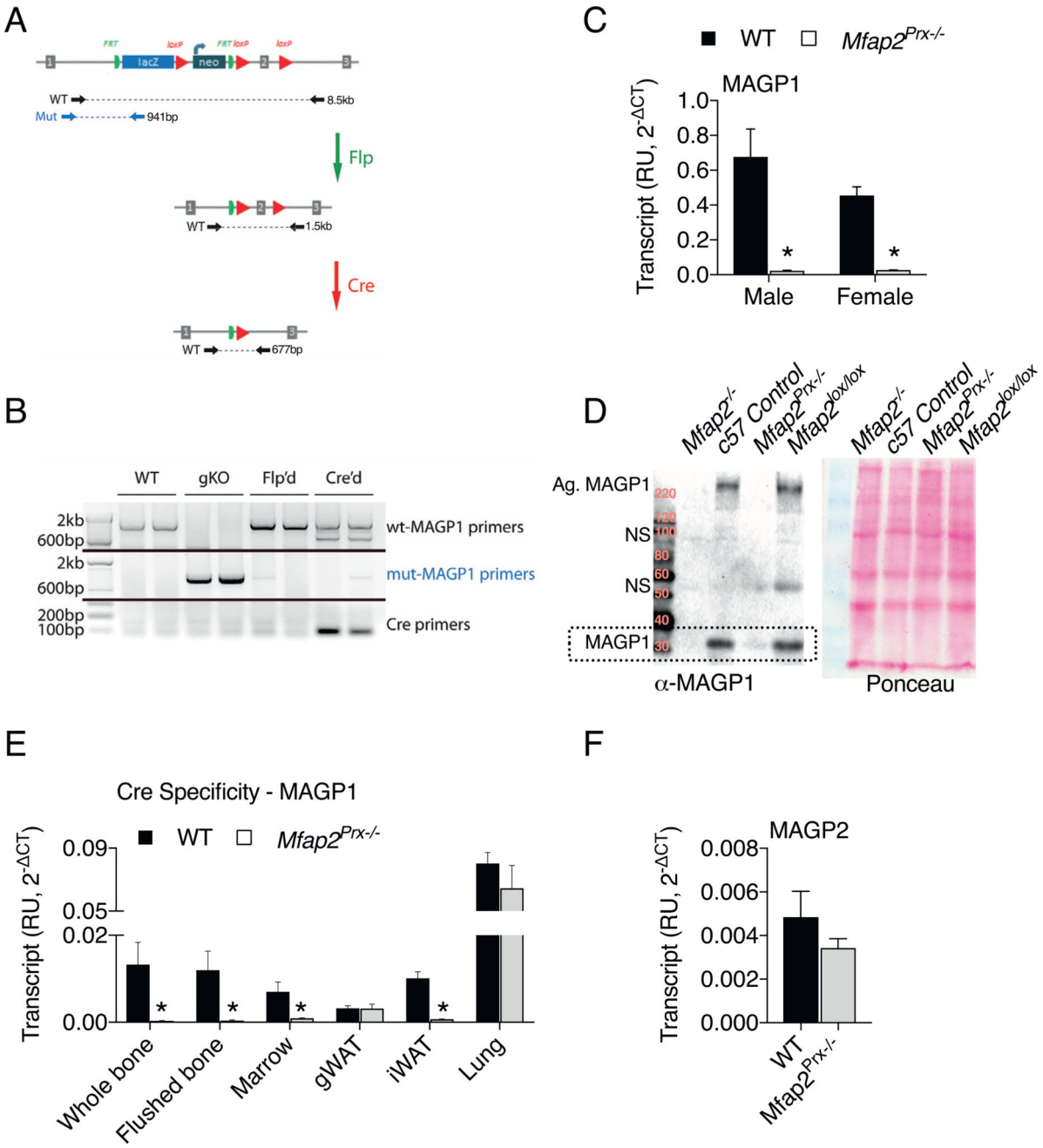

Fig. 1.

Mfap2$^{lox/lox}$ construct design, genotyping and MAGP1 expression. 1A) Breeding strategy and schematic of flox'd *Mfap2* construct, showing Frt (green) flanking the neo cassette, and loxP sites (red) flanking exon 2 of *Mfap2*. The schematic also shows the construct following flipase (Flp)-mediated removal of the neo cassette (restoring MAGP1 expression), then the construct following Cre-mediated excision of exon 2 for conditional deletion of *Mfap2*. Genotyping required the use of three primer sets. “WT” primers are in the introns of the Mfap2 gene flanking exon 2 (outside the construct). “Mut” primers utilized a sequence found only in the *Mfap2*$^{lox/lox}$ cassette. ‘Cre’ primers are necessary for detection of the

Prx1-Cre transgene. The location of the 'WT' and 'Mut' primers used for genotyping are indicated by black and blue arrows respectively. 1B) Genotyping strategy demonstrated on whole tibia samples. 1C) Prx1-Cre efficiency in male and female bones. RT-qPCR on RNA from whole femurs, using TaqMan primer-probes demonstrates efficient deletion of Mfap2 transcript by one copy of the Prx1-Cre transgene (N = 6). 1D). Western immunoblot of whole bone protein lysates to show loss ofMAGP1 protein in the presence of the Prx1-Cre. Whole blot is shown for visualization of MAGP1 monomers (~35 kDa, boxed), non-specific bands (NS, ~55 kDa & 80 kDa), and aggregated MAGP1 (Ag. MAGP1, >220 kDa). Protein marker (kDa) is also shown. Ponceau stain was used prior to antibody incubation to confirm equal protein loading. 1E) MAGP1 transcript expression was measured using TaqMan primer-probe sets and TaqMan universal master mix as in 1C, across several tissue types demonstrating the specificity of the Prx1-Cre (N = 4). 1F) MAGP2 (*Mfap5*) expression in whole tibia was similarly assessed using TaqMan primer-probe sets (N = 4). Control (WT) mice are $Mfap2^{lox/lox}$ littermates. iWAT is inguinal white adipose tissue. gWAT is gonadal white adipose tissue. Student's *t*-test was used to make single comparison between control and Cre-positive samples, * = $p < 0.05$. Data shown as mean +/− SEM. (For interpretation of the references to colour in this figure legend, the reader is referred to the web version of this article.)

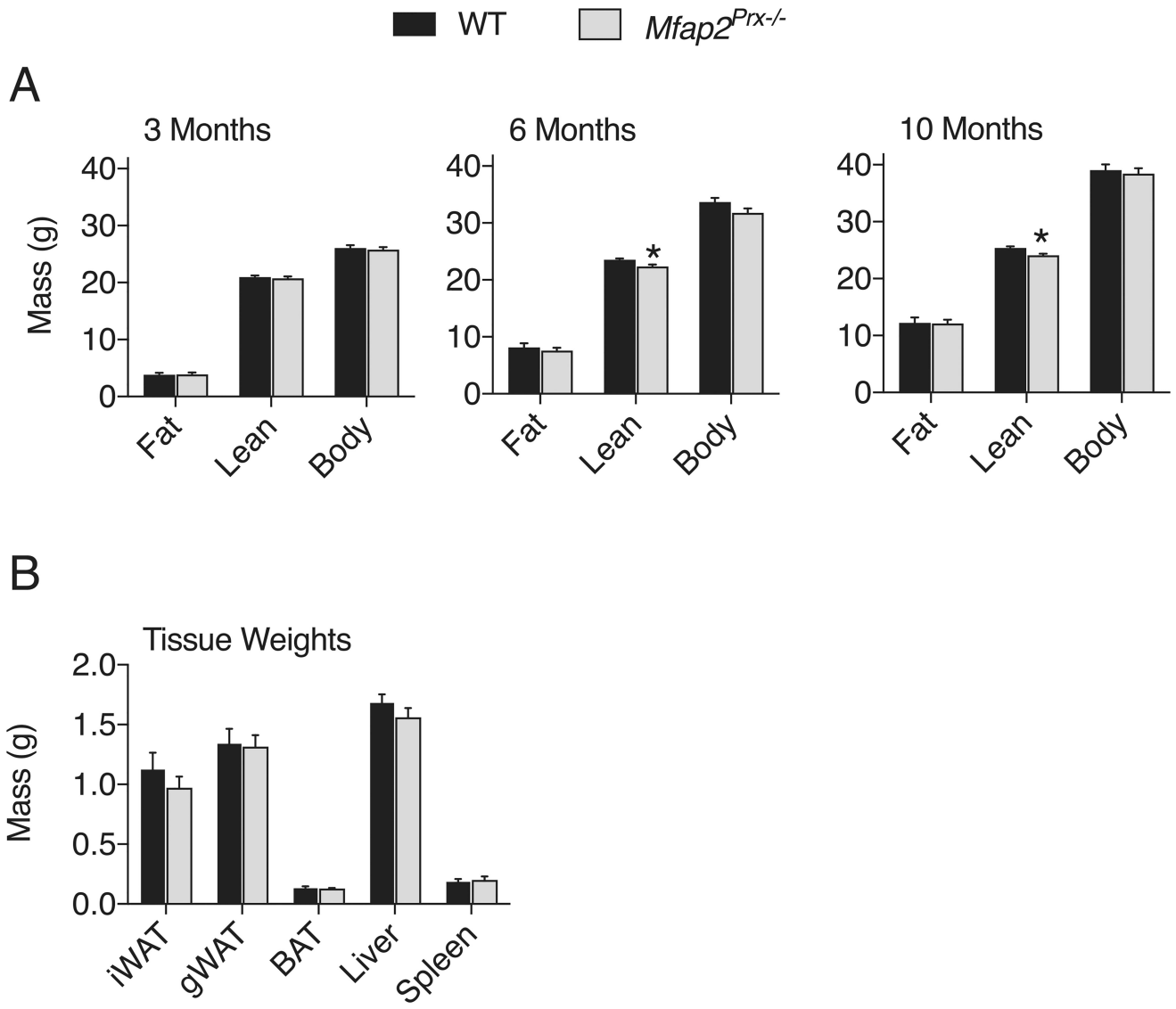

Fig. 2.

Prx1-mediated deletion of MAGP1 has no consequence on whole body adiposity. 2A) Serial EchoMRI was performed to determine whole body composition on control and Cre + mice at 3-, 6-, and 10-months of age (N = 14 for WT and 10 for Cre+). 2B) Wet tissue weights were determined at time of dissection (10-months old, N = 14,10). Control (WT) mice are *Mfap2*$^{lox/lox}$ littermates. Student's t-test was used for single comparisons between control and Cre-positive samples, * = $p < 0.05$, all mice were male. Data shown as mean +/− SEM.

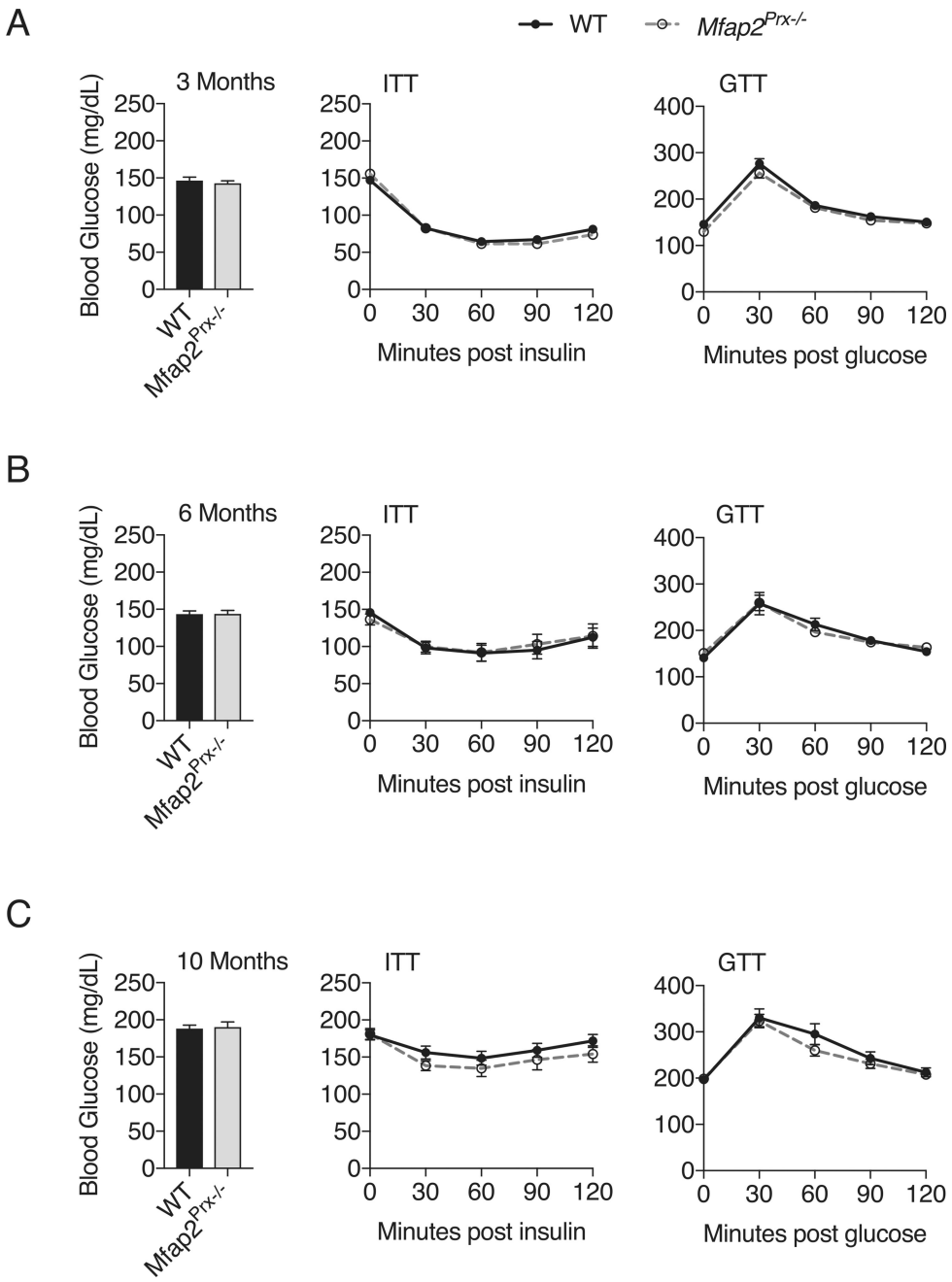

Fig. 3.

Prx1-mediated deletion of MAGP1 has no consequence on insulin sensitivity or glucose disposal. Serial fasted glucose, insulin tolerance (ITT) and glucose tolerance (GTT) tests were performed at 3- (A), 6- (B), and 10- (C) months of age. All tests were performed following a 6-hour daytime fast. For ITT, mice received a 0.75 U/kg insulin bolus i.p. For GTT, mice received a 1 mg/g dextrose bolus i.p. Blood glucose was determined using Bayer meters and tail blood. N = 14,10. Student's *t*-test was used for comparison of fasted glucose measure. Control (WT) mice are *Mfap2*$^{lox/lox}$ littermates. Two-way ANOVA was used to

determine whether genotype effected insulin sensitivity or glucose clearance over time. No statistical differences were found. All mice were male. Data shown as mean +/− SEM.

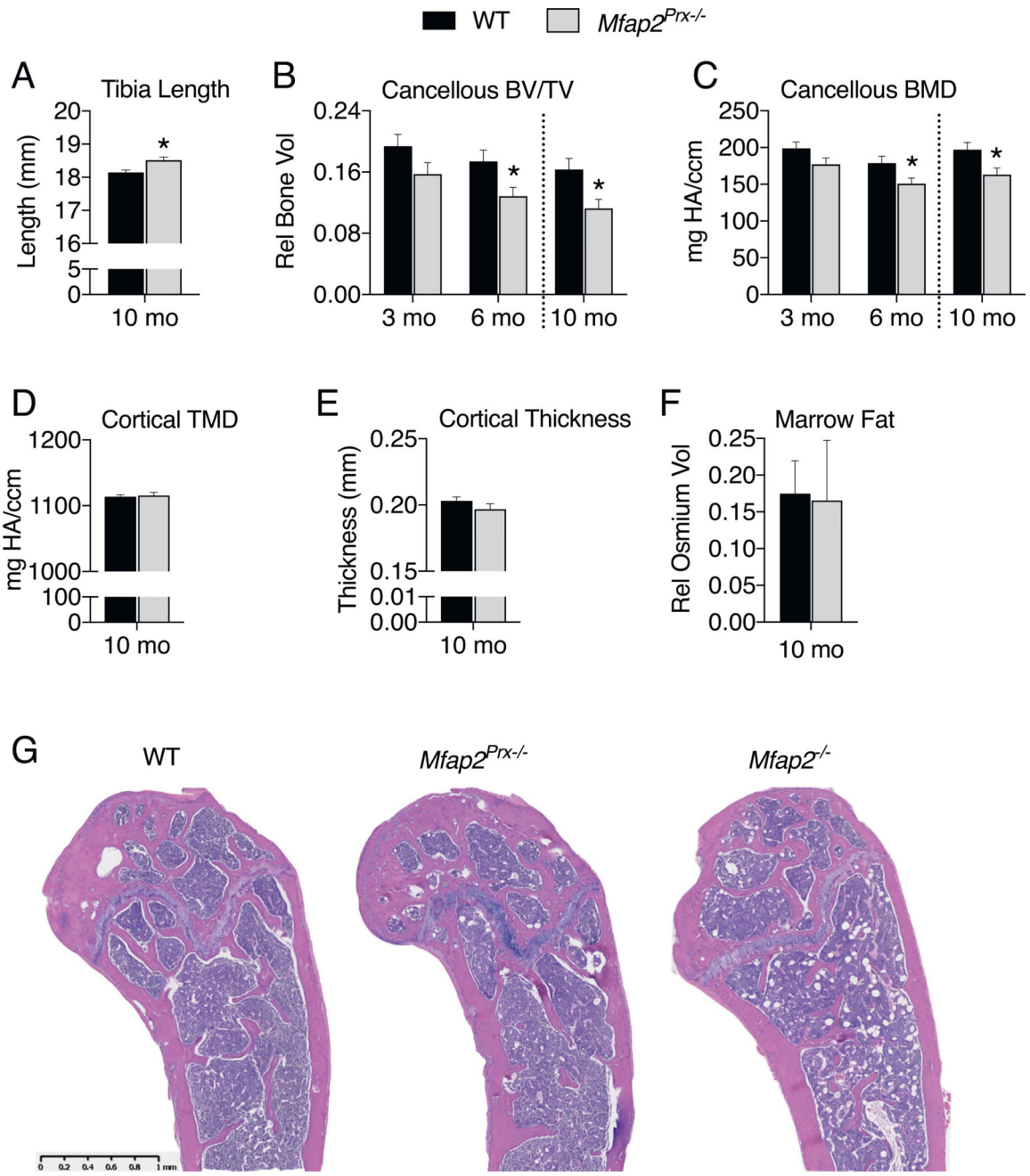

Fig. 4.

Prx1-mediated deletion of MAGP1 results in long bone overgrowth and reduced bone mass. 4A) Digital caliper was used to determine tibia length (N = 14,10). 4B–E) Bone volume and mineral density of tibias were determined by computed tomography. VivaCT was used at 3- and 6- months was conducted on live mice (cancellous bone only). MicroCT was used to scan dissected 10-month-old tibias (cancellous and cortical bone). Energy and resolution settings were equivalent between machines. Student *t*-tests were used for comparison of control and Cre + animals at each age, statistical significance ($p < 0.05$) is indicated by *. Two-way ANOVA was used to determine whether genotype effected cancellous bone

volume/total volume (BV/TV) and bone mineral density (BMD) over time. Statistical significance was achieved (N = 14,10). 4F) Bone marrow adiposity was determined on decalcified, osmium-stained tibias. Data shown is the volume of osmium (fat) relative to the marrow cavity volume (determined from calcified bone scan). N = 14,10. 4G) Representative images of H&E stained tibias from Cre- control (WT), Prx1-Cre + (*Mfap2*$^{Prx-/-}$) and MAGP1 germline knockout (*Mfap2*$^{-/-}$) mice (N = 3,4,3). Control (WT) mice are *Mfap2*$^{lox/lox}$ littermates. All mice were male. Data shown as mean +/− SEM.

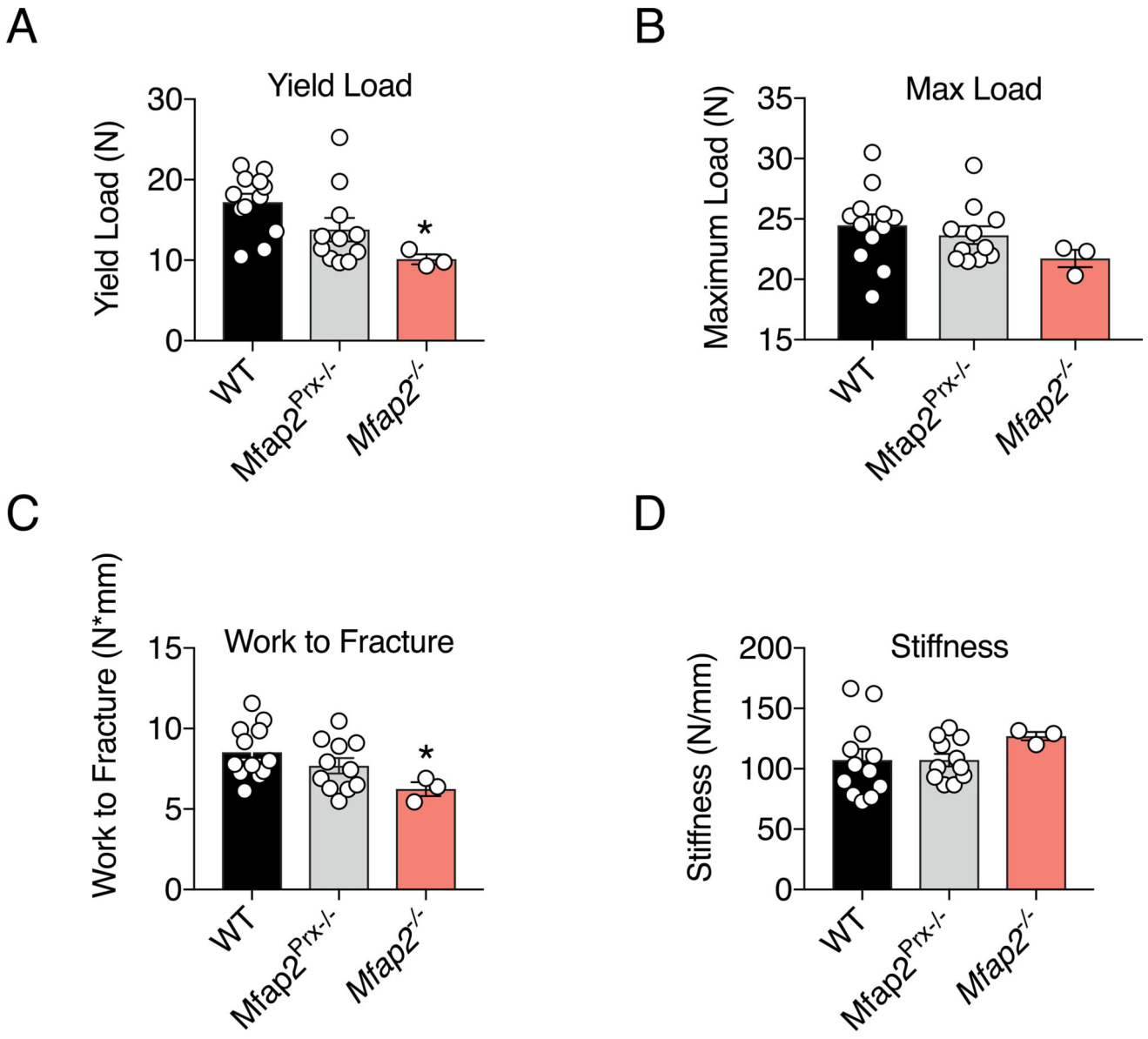

Fig. 5.

Germline MAGP1 deficiency but not local deficiency (Prx1-mediated) causes reduced bone mechanical properties. Hydrated femurs from 10-month-old mice were subjected to 3-point bend testing. One-way ANOVA was used to compare parameters amongst genotype. * indicates germline knockout mice (*Mfap2*$^{-/-}$) were significantly different ($p < 0.05$) from WT (Cre-) bones. N = 12,11,3. Control (WT) mice are *Mfap2*$^{lox/lox}$ littermates. All mice were male. Data shown as mean +/− SEM.

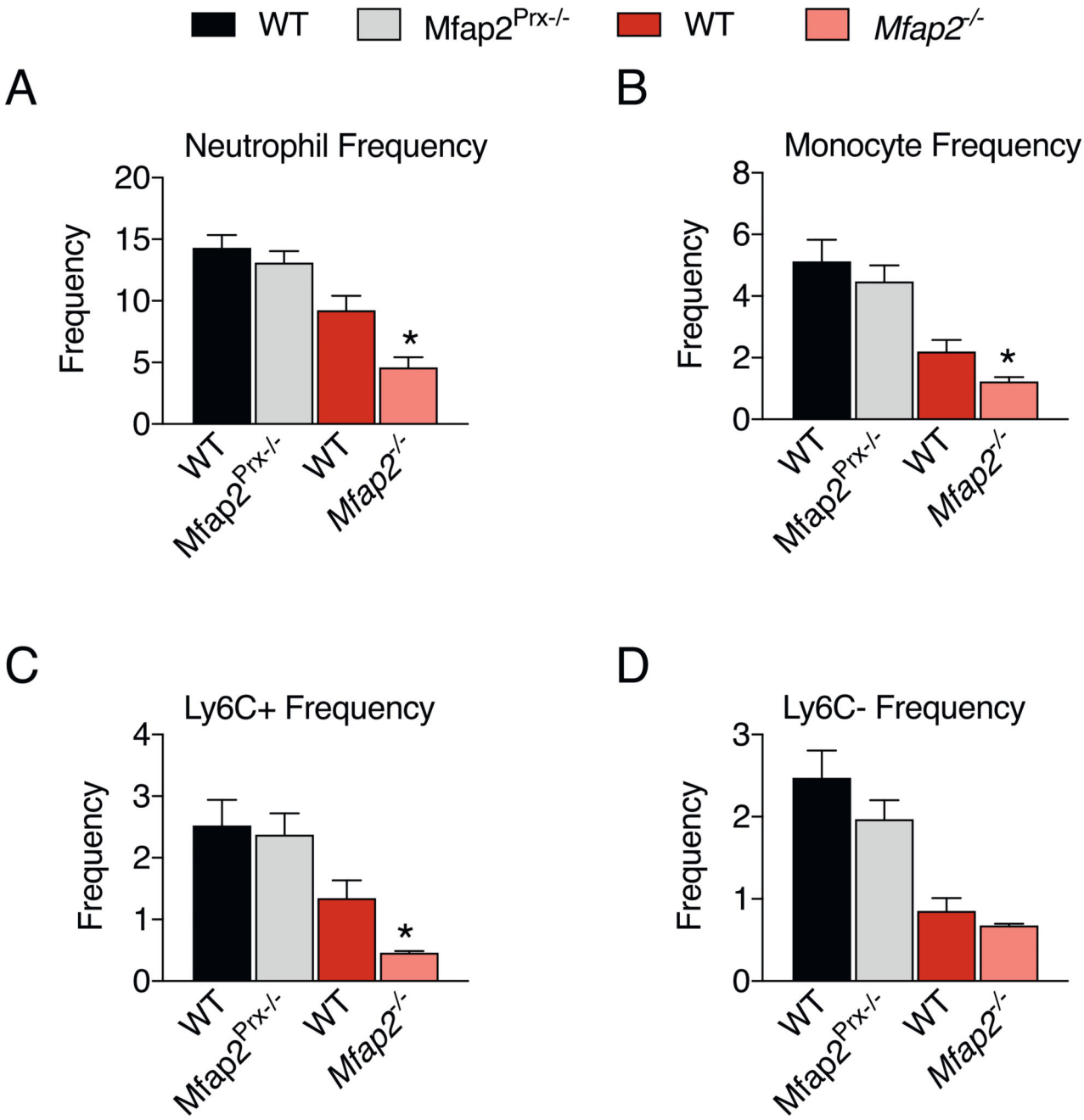

Fig. 6.

Germline MAGP1 deficiency but not local deficiency (Prx1-mediated) causes neutropenia and monocytopenia. Flow cytometry was used to determine neutrophil and monocyte frequency in blood. Students t-test was used to compare mutant mice to their own control (WT) mice (* = $p < 0.05$, N for 4A & 4B = 11,11,13, 11; N for 4C & 4D = 6,4,13,11). All mice were male. Data shown as mean +/− SEM.

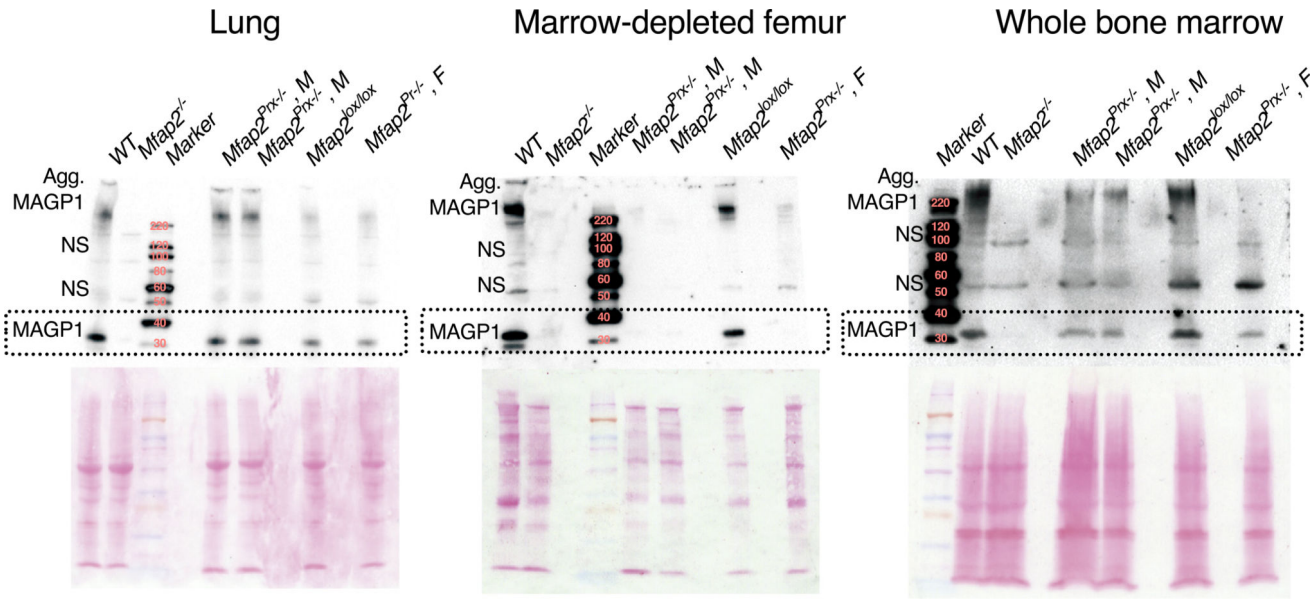

Fig. 7.

MAGP1 protein accumulates in MAGP1 transcript-deficient bone marrow samples. SDS-PAGE immunoblots with MAGP1 targeted antibody show the presence, or absence, of MAGP1 protein in tissue lysates from lung, marrow-depleted bone (femur) or whole bone marrow. C57BL/6J mice (WT) and germline MAGP1 knockout (*Mfap2*$^{-/-}$, KO) mice served as positive and negative controls for the MAGP1 antibody. Prx1-Cre-mediated deletion was assessed in male and female mice (*Mfap2*$^{Prx-/-}$, M or *Mfap2*$^{Prx-/-}$, F). Cre-negative (*Mfap2*$^{lox/lox}$) tissue served as a second positive control for MAGP1 protein detection. Whole blot is shown for visualization of MAGP1 monomers (~35 kDa, boxed), non-specific bands (NS, ~55 kDa & 80 kDa), and aggregated MAGP1 (Ag. MAGP1, >220 kDa). Protein marker (kDa) is also shown.

Table 1

µCT analysis of WT and *Mfap2*$^{Prx-/-}$ cancellous bone.

Parameter		3 months		6 months		10 months	
	Genotype	Mean	p value	Mean	p value	Mean	p value
Total volume (TV, mm^3)	WT	1.90 ± 0.047	**0.002**	1.83 ± 0.035	**5.78E-05**	1.91 ± 0.038	**3.97E-04**
	Cre +	1.65 ± 0.050		1.59 ± 0.031		1.66 ± 0.047	
Bone volume (BV, mm^3)	WT	0.36 ± 0.025	**0.010**	0.32 ± 0.026	**0.004**	0.31 ± 0.027	**0.003**
	Cre +	0.26 ± 0.027		0.20 ± 0.020		0.19 ± 0.022	
Bone volume/total volume (BV/TV)	WT	0.19 ± 0.015	0.110	0.17 ± 0.015	**0.035**	0.16 ± 0.014	**0.017**
	Cre +	0.16 ± 0.015		0.13 ± 0.012		0.11 ± 0.012	
Connectivity density	WT	94.02 ± 8.87	0.123	49.08 ± 5.52	**0.023**	31.16 ± 4.18	**0.050**
	Cre +	71.87 ± 10.64		30.78 ± 4.33		19.67 ± 2.90	
Structure model index	WT	2.68 ± 0.100	0.063	2.50 ± 0.134	**0.047**	2.33 ± 0.140	**0.013**
	Cre +	2.99 ± 0.131		2.89 ± 0.114		2.92 ± 0.163	
Trabecular number	WT	5.52 ± 0.149	0.161	4.55 ± 0.124	**0.032**	3.77 ± 0.132	0.217
	Cre +	5.18 ± 0.178		4.16 ± 0.097		3.51 ± 0.158	
Trabecular thickness (mm)	WT	0.06 ± 0.002	0.098	0.06 ± 0.002	**0.049**	0.07 ± 0.022	**0.019**
	Cre +	0.05 ± 0.002		0.06 ± 0.002		0.06 ± 0.022	
Trabecular separation (mm)	WT	0.18 ± 0.006	0.160	0.22 ± 0.007	**0.029**	0.27 ± 0.010	0.196
	Cre +	0.19 ± 0.008		0.24 ± 0.006		0.29 ± 0.018	
Bone mineral density (mg HA/ccm)	WT	198.77 ± 8.72	0.104	178.70 ± 9.52	**0.044**	197.08 ± 9.65	**0.022**
	Cre +	177.31 ± 8.61		150.97 ± 7.61		163.25 ± 8.87	

Bold data indicate significance at p value < 0.05.

Table 2

µCT analysis of WT and *Mfap2*$^{Prx-/-}$ cortical bone.

Parameter	10 months		
	Genotype	**Mean**	**p value**
Cortical bone thickness (mm)	WT	0.202 ± 0.003	0.864
	Cre +	0.201 ± 0.004	
Tissue mineral density (mg HA/ccm)	WT	1114 ± 2.77	0.713
	Cre +	1117 ± 4.82	
Total area (mm^2)	WT	1.35 ± 0.022	0.188
	Cre +	1.29 ± 0.039	
Bone area (mm^2)	WT	0.73 ± 0.017	0.554
	Cre +	0.71 ± 0.026	
Medullary area (mm^2)	WT	0.62 ± 0.010	**0.003**
	Cre +	0.58 ± 0.017	
Polar moment of inertia [mm^4]	WT	0.22 ± 0.009	0.292
	Cre +	0.20 ± 0.013	

Table 3

Frequency of blood cell types by flow cytometry.

Parameter	Male *Mfap2*$^{Prx-/-}$			Female *Mfap2*$^{Prx-/-}$			*Mfap2*$^{-/-}$		
	Genotype	Mean	p value	Genotype	Mean	p value	Genotype	Mean	p value
Blood count Ab#	WT	7.96 ± 0.63E+06	0.314	WT	7.65 ± 0.71E+06	0.925	WT	3.43 ± 0.84E+05	**0.020**
	Cre+	8.91 ± 0.67E+06		Cre+	7.78 ± 0.50E+06		*Mfap2*$^{-/-}$	1.21 ± 0.33E+06	
Neutrophil	WT	14.31 ± 1.02	0.404	WT	15.63 ± 0.96	0.633	WT	9.24 ± 1.16	**0.004**
	Cre+	13.12 ± 0.94		Cre+	16.85 ± 3.55		*Mfap2*$^{-/-}$	4.60 ± 0.83	
Eosinophil	WT	1.84 ± 0.38	0.571	WT	2.55 ± 0.30	0.476	WT	–	–
	Cre+	1.51 ± 0.46		Cre+	2.05 ± 0.77		*Mfap2*$^{-/-}$	–	
Monocyte	WT	5.13 ± 0.70	0.475	WT	5.44 ± 0.69	0.672	WT	2.20 ± 0.37	**0.026**
	Cre+	4.47 ± 0.53		Cre+	6.08 ± 1.41		*Mfap2*$^{-/-}$	1.23 ± 0.14	
Ly6C+ Monocyte	WT	2.53 ± 0.42	0.790	WT	3.18 ± 0.51	0.914	WT	1.35 ± 0.28	**0.037**
	Cre+	2.38 ± 0.34		Cre+	3.29 ± 0.64		*Mfap2*$^{-/-}$	0.46 ± 0.02	
Lyc6− Monocyte	WT	2.48 ± 0.33	0.238	WT	2.24 ± 0.23	0.396	WT	0.85 ± 0.16	0.398
	Cre+	1.97 ± 0.23		Cre+	2.74 ± 0.75		*Mfap2*$^{-/-}$	0.68 ± 0.02	
B Cell	WT	48.72 ± 1.64	0.616	WT	37.13 ± 2.69	0.476	WT	55.75 ± 2.09	0.058
	Cre+	50.2 ± 2.53		Cre+	41.75 ± 7.55		*Mfap2*$^{-/-}$	62.425 ± 1.90	
T Cell	WT	17.62 ± 0.91	0.68	WT	25.48 ± 1.65	0.242	WT	25.9 ± 2.51	0.269
	Cre+	18.4 ± 1.72		Cre+	21.55 ± 0.75		*Mfap2*$^{-/-}$	21.98 ± 1.29	
CD8 T Cell	WT	8.30 ± 0.51	0.559	WT	13.03 ± 0.82	0.083	WT	11.70 ± 0.84	0.636
	Cre+	8.87 ± 0.88		Cre+	9.94 ± 0.01		*Mfap2*$^{-/-}$	11.12 ± 0.67	
CD4 T Cell	WT	8.69 ± 0.54	0.831	WT	11.34 ± 1.38	0.874	WT	13.14 ± 1.98	0.279
	Cre+	8.91 ± 0.96		Cre+	10.91 ± 1.19		*Mfap2*$^{-/-}$	10.20 ± 0.73	

Table 4

Frequency of bone marrow cell types by flow cytometry.

Parameter	Male *Mfap2*$^{Prx-/-}$		
	Genotype	**Mean**	**p value**
Bone marrow cell count	WT	2.79 ± 0.15 E+07	0.346
	Cre+	2.96 ± 0.08 E+07	
CDP	WT	0.05 ± 0.008	0.075
	Cre+	0.03 ± .005	
MDP	WT	0.03 ± 0.008	0.410
	Cre+	0.02 ± 0.003	
MP	WT	0.15 ± 0.017	0.804
	Cre+	0.15 ± 0.009	
PreDC	WT	0.18 ± 0.026	0.785
	Cre+	0.17 ± 0.011	
Neutrophil	WT	23.02 ± 1.514	0.508
	Cre+	25.68 ± 3.530	
Ly6C+ Mono	WT	7.84 ± 0.503	0.709
	Cre+	7.60 ± 0.372	
Ly6C− Mono	WT	0.45 ± 0.080	0.365
	Cre+	0.37 ± 0.034	